Journal of Power Sources 196 (2011) 8809–8814

Contents lists available at ScienceDirect

Journal of Power Sources

journal homepage: www.elsevier.com/locate/jpowsour

The electrochemical behaviors of Mg, Mg–Li–Al–Ce and Mg–Li–Al–Ce–Y in sodium chloride solution

Yanzhuo Lv[a,*], Yan Xu[b], Dianxue Cao[a]

[a] Key Laboratory of Superlight Material and Surface Technology of Ministry of Education, College of Material Science and Chemical Engineering, Harbin Engineering University, Harbin 150001, PR China
[b] Engineering Training Center, Harbin Engineering University, Harbin 150001, PR China

ARTICLE INFO

Article history:
Received 9 October 2010
Received in revised form 26 May 2011
Accepted 1 June 2011
Available online 12 June 2011

Keywords:
Magnesium
Magnesium–lithium–aluminum–cerium
Magnesium–lithium–aluminum–cerium–yttrium
Anode
Magnesium–hydrogen peroxide semi-fuel cells

ABSTRACT

The electrochemical performances of magnesium, magnesium–lithium–aluminum–cerium and magnesium–lithium–aluminum–cerium–yttrium as the anode of magnesium–hydrogen peroxide semi-fuel cells have been studied by methods of potentiodynamic, potentiostatic and electrochemical impedence measurements. The surface morphologies of magnesium and its alloys have been examined by scanning electron microscopy (SEM). It has been found that magnesium–lithium–aluminum–cerium and magnesium–lithium–aluminum–cerium–yttrium electrodes are less corrosion resistant than that of magnesium electrode in 0.7 mol L^{-1} NaCl solution and the corrosion current density decreases with the following order: magnesium < magnesium–lithium–aluminum–cerium–yttrium < magnesium–lithium–aluminum–cerium. The magnesium–lithium–aluminum–cerium–yttrium anode is more active than magnesium–lithium–aluminum–cerium and magnesium. The magnesium–hydrogen peroxide semi-fuel cell with magnesium–lithium–aluminum–cerium–yttrium anode shows better performance than that with Mg–Li–Al–Ce and Mg.

1. Introduction

Metal-hydrogen peroxide semi-fuel cells exhibit many potential advantages, such as low cost, environmentally benign, stable discharge voltage, high power density and high specific energy. They have been studied as the power sources for long endurance unmanned underwater vehicles [1–10]. This electrochemical system consists of a metal anode, a conductive membrane and a cathode catalyst. Mg as an attractive anode material has received the recent attention because it has high Faradic capacity (2.2 Ah g^{-1}), high specific energy (6.8 kWh kg^{-1}) and more negative standard reduction potential (−2.37 V vs. standard hydrogen electrode (SHE)) [11]. In addition, Mg–H_2O_2 semi-fuel cell has a theoretical voltage of 4.14 V, which is higher than that of Al–H_2O_2 semi-fuel cell [12,13] and Al–AgO battery. Thus, Mg–H_2O_2 semi-fuel cell is a promising power source with the high energy density for undersea water applications. The theoretical anode, cathode and cell reactions as well as the potentials for Mg–H_2O_2 semi-fuel cell [14–17] are as follows (Eqs. (1)–(3)):

$$\text{Anode}: \quad Mg \rightarrow Mg^{2+} + 2e^-, \quad E^0 = 2.37\,V \quad \text{vs. SHE} \tag{1}$$

$$\text{Cathode}: \quad H_2O_2 + 2H^+ + 2e^- \rightarrow 2H_2O, \quad E^0 = 1.77\,V \quad \text{vs. SHE} \tag{2}$$

$$\text{Cell}: \quad Mg + H_2O_2 + 2H^+ \rightarrow Mg^{2+} + 2H_2O, \quad E_{cell} = 4.14\,V \tag{3}$$

However, in practical system, the following reactions (Eqs. (4)–(7)) would lead to the decrease in the performance of the Mg anode and then Mg–H_2O_2 semi-fuel cell.

The decomposition reaction:

$$2H_2O_2 \rightarrow 2H_2O + O_2 \uparrow \tag{4}$$

The deposition reactions:

$$Mg^{2+} + 2OH^- \rightarrow Mg(OH)_2(s) \tag{5}$$

$$Mg^{2+} + CO_3^{2-} \rightarrow MgCO_3(s) \tag{6}$$

The direct reaction:

$$Mg + H_2O_2 + 2H^+ \rightarrow Mg^{2+} + 2H_2O \tag{7}$$

It was reported [12,18,19] that two approaches could solve the above problems. One is using the Mg alloys as the anode materials or using the anode materials with the high surface area, such as granular metal anode [19]. The other is using additives

* Corresponding author. Tel.: +86 15304666692; fax: +86 451 82589036.
E-mail address: lvyanzhuo@hrbeu.edu.cn (Y. Lv).

0378-7753/$ – see front matter © 2011 Elsevier B.V. All rights reserved.
doi:10.1016/j.jpowsour.2011.06.001

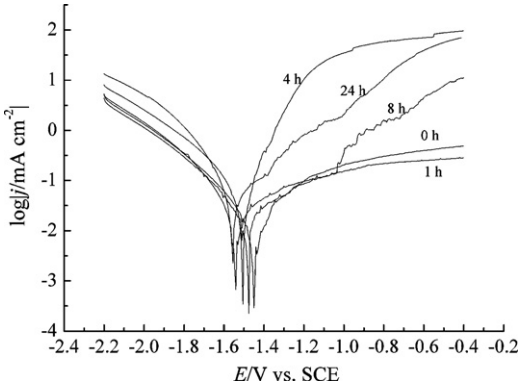

Fig. 1. The Tafel plot of the Mg electrode in 0.7 mol L^{-1} NaCl solution after soaking in 0.7 mol L^{-1} NaCl solution for different soaking times.

in the electrolyte to activate the anode or to inhibit the formation of the oxide film on the anode. Sivashanmugam et al. [20] investigated the possibility of Mg–Li alloy (with 13 wt.% Li) as the anode in magnesium primary reserve batteries. The Mg–Li alloy anode exhibits an anodic efficiency of 81% at the current density of 8.6 mA cm^{-2}. Especially, the Mg–Li/$MgCl_2$/CuO battery can offer the higher operating voltage and capacity than that of the battery with the Mg–Al alloy anode. Lin et al. [21] investigated the electrochemical behavior and corrosion performance of Mg–Li–Al–Zn anodes with high Al composition. They found that the Mg–Li–Al–Zn alloy with ~9 wt.% Al has the high discharge voltage in $MgCl_2$ electrolyte. Cao et al. [22–24] investigated the electrochemical behavior of Mg–Li, Mg–Li–Al, Mg–Li–Al–Ce, Mg–Li–Al–Sn, Mg–Li–Al–Ce–Sn, Mg–Li–Al–Ce–Zn, and Mg–Li–Al–Ce–Zn–Mn in 0.7 mol L^{-1} NaCl solution. They found that the alloying elements of Al, Ce, Sn, Zn, and Mn have significant effects on the discharging current densities and the utilization efficiencies of the alloys. Ce can enhance both the discharge activity and utilization efficiency. Sn mainly improves the discharge current.

In this article, in order to understand the effect of the alloy element of Y on the electrochemical performance of the Mg–Li–Al–Ce alloy, the electrochemical behaviors of Mg–Li–Al–Ce and Mg–Li–Al–Ce–Y alloys in 0.7 mol L^{-1} NaCl solution were investigated. The performances of Mg–H_2O_2 semi-fuel cell using the above alloys as anodes were compared.

2. Experimental

Mg–Li–Al–Ce and Mg–Li–Al–Ce–Y alloys were prepared by vacuum melting method. The ingots of pure magnesium (99.99%), pure lithium (99.99%), pure aluminum (99.99%), Mg–Ce alloy containing 20.63 wt.% Ce and Mg–Y alloys containing 19 wt.% Y were put into the vacuum induction melting furnace according to the composition of the alloys under the protection of ultrahigh purity argon, and the furnace was then evacuated to 1.0×10^{-2} Pa. After the furnace was charged with high purity argon, the temperature of the furnace was raised to melt the magnesium and the alloying components. Then the molten alloys were poured into a stainless steel mold and cooled down to room temperature under the protection of argon. The composition of the Mg alloys was listed in Table 1.

Table 1
Nominal composition of the alloys (wt.%).

Alloys	Mg	Li	Al	Ce	Y
Mg–Li–Al–Ce	87.1	8.5	3.2	1.2	–
Mg–Li–Al–Ce–Y	85.9	8.5	3.2	1.2	1.2

Table 2
The corrosion parameters of the Mg electrode measured after soaked in 0.7 mol L^{-1} NaCl solution for different periods.

Soaked time (h)	Corrosion potential (V)	Corrosion current density (μA cm^{-2})	Open circuit potential (V)
0	−1.495	44.3	−1.695
1	−1.510	46.8	−1.682
4	−1.524	21.3	−1.642
8	−1.531	19.0	−1.621
24	−1.553	12.9	−1.579

Electrochemical measurements were carried out in the homemade three electrode electrochemical cell [23]. The saturated calomel electrode (SCE) was used as the reference electrode. All the potentials were quoted with respect to SCE. The platinum foil and Mg (Mg alloys) were used as the counter electrode and the working electrode, respectively. The apparent surface area of the working electrode is 0.95 cm^2. Prior to use, the working electrode was successively polished with 120#, 360# and 700# metallographic emery papers, washed with deoxygenated ultrapure water (Milli-Q), degreased with acetone and rinsed with deoxygenated ultrapure water again. The electrolyte is 0.7 mol L^{-1} NaCl solution. It was purged with N_2 gas for 15 min before measurements in order to remove the O_2 gas dissolved in the solution.

The electrochemical experiments were performed using a VMP3/Z potentiostat (Bio-logic). The potential for Tafel plot was −2.2 to −0.4 V vs. SCE and the scanning rate was 5 mV s^{-1}. Potentiostatic current–time curves were tested at −1.0 V for 5 min. Electrochemical impedance spectra were recorded under open circuit potentials with the frequency range from 1 to 200,000 Hz with

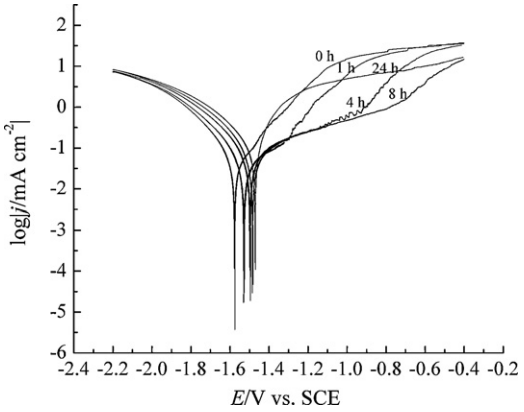

Fig. 2. The Tafel plot of the Mg–Li–Al–Ce electrode in 0.7 mol L^{-1} NaCl solution after soaking in 0.7 mol L^{-1} NaCl solution for different soaking times.

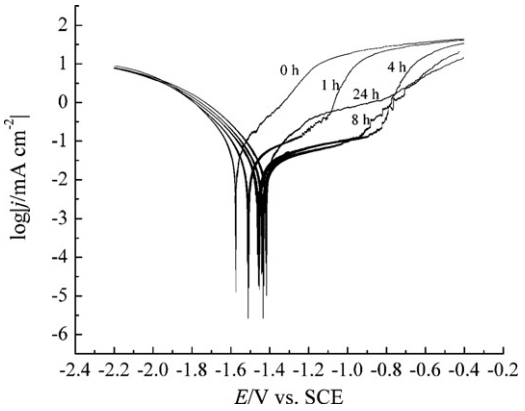

Fig. 3. The Tafel plot of the Mg–Li–Al–Ce–Y electrode in 0.7 mol L^{-1} NaCl solution after soaking in 0.7 mol L^{-1} NaCl solution for different soaking times.

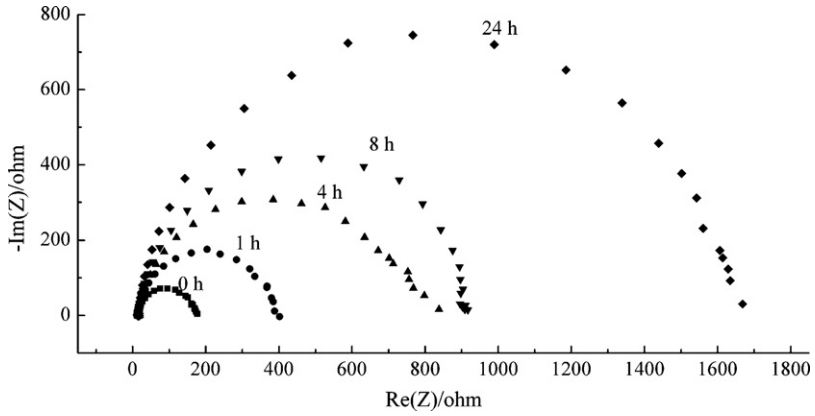

Fig. 4. The impedance spectra of the Mg electrode recorded after soaking in 0.7 mol L^{-1} NaCl solution for different soaking times.

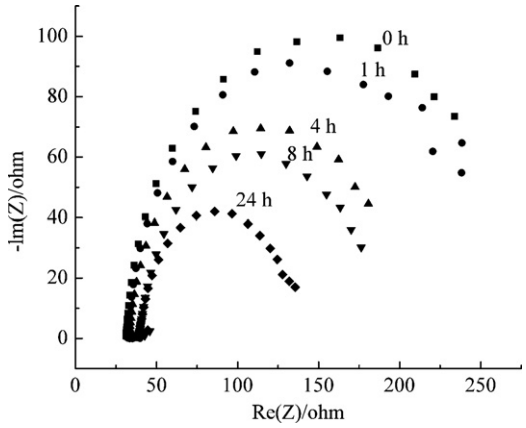

Fig. 5. The impedance spectra of the Mg–Li–Al–Ce electrode recorded after soaking in 0.7 mol L^{-1} NaCl solution for different soaking times.

the amplitude of 8 mV. The morphology of the electrode surface was examined using scanning electron microscopy (SEM; JSM-S4800) equipped with energy dispersive spectroscopy (EDS unit). The images were acquired using a 20 kV accelerating voltage.

3. Results and discussion

Fig. 1 shows the Tafel plot of E vs. $\log i$ of the Mg electrode after the Mg electrode was soaked in 0.7 mol L^{-1} NaCl solution for different times. Table 2 displays the corrosion parameters of the Mg electrode measured after soaked in 0.7 mol L^{-1} NaCl solution for the different soaking times. It can be observed from Fig. 1 and Table 2 that the corrosion current density of the Mg electrode decreases with the soaking times. However, Mg–Li–Al–Ce and Mg–Li–Al–Ce–Y alloys display different performance as seen from Fig. 2 (Table 3) and Fig. 3 (Table 4). The corrosion current den-

Table 3
The corrosion parameters of Mg–Li–Al–Ce electrode measured after soaked in 0.7 mol L^{-1} NaCl solution for different periods.

Soaked time (h)	Corrosion potential (V)	Corrosion current density (μA cm^{-2})	Open circuit potential (V)
0	−1.636	52.8	−1.644
1	−1.510	43.3	−1.619
4	−1.493	60.5	−1.600
8	−1.472	66.2	−1.598
24	−1.520	168.2	−1.595

Table 4
The corrosion parameters of Mg–Li–Al–Ce–Y electrode measured after soaked in 0.7 mol L^{-1} NaCl solution for different periods.

Soaked time (h)	Corrosion potential (V)	Corrosion current density (μA cm^{-2})	Open circuit potential (V)
0	−1.568	36.2	−1.666
1	−1.501	34.6	−1.615
4	−1.454	22.8	−1.607
8	−1.433	21.8	−1.605
24	−1.439	35.1	−1.603

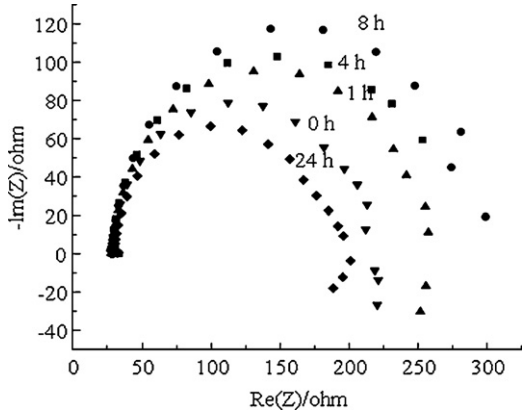

Fig. 6. The impedance spectra of the Mg–Li–Al–Ce–Y electrode recorded after soaking in 0.7 mol L^{-1} NaCl solution for different soaking times.

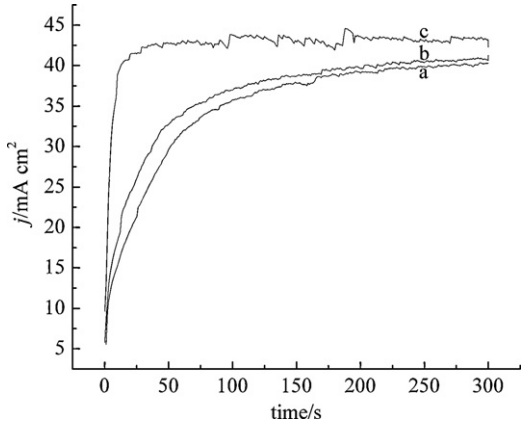

Fig. 7. The chronoamperometric curves of (a) Mg, (b) Mg–Li–Al–Ce and (c) Mg–Li–Al–Ce–Y electrodes at −1.0 V in 0.7 mol L^{-1} NaCl solution.

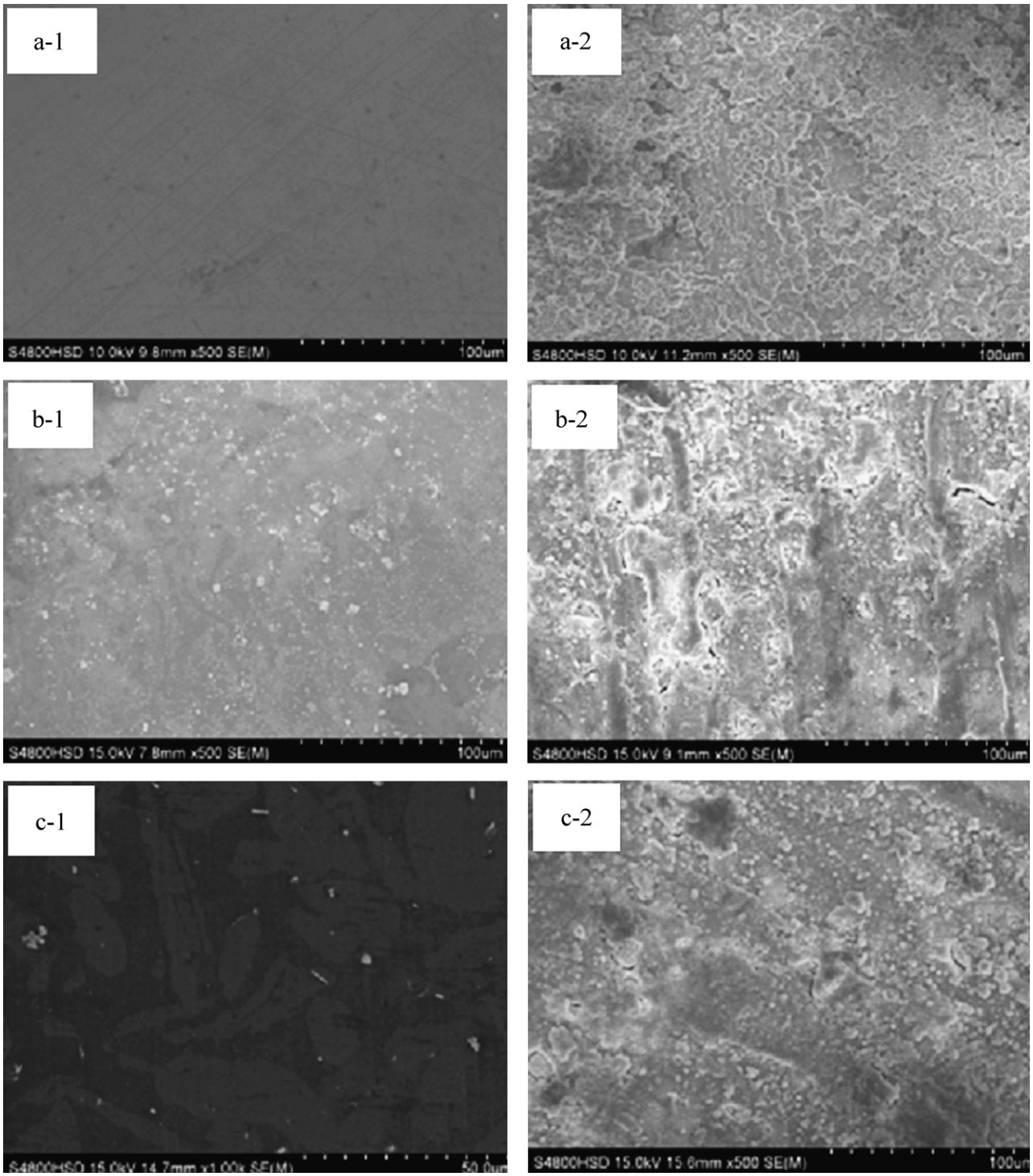

Fig. 8. The SEM photographs of (a) Mg, (b) Mg–Li–Al–Ce and (c) Mg–Li–Al–Ce–Y electrodes (1) before and (2) after soaking in 0.7 mol L^{-1} NaCl solution for 8 h.

sities of the Mg–Li–Al–Ce and Mg–Li–Al–Ce–Y electrodes decrease firstly and then increase with the increase in the soaking time. After soaking for 24 h, the Mg, Mg–Li–Al–Ce and Mg–Li–Al–Ce–Y electrode present a corrosion current of 12.9 μA cm^{-2}, 168.2 μA cm^{-2} and 35.1 μA cm^{-2}, respectively. It indicates that Mg is more corrosion resistive than Mg–Li–Al–Ce–Y and Mg–Li–Al–Ce alloys and the corrosion resistive order decreases in the following sequence: Mg > Mg–Li–Al–Ce–Y > Mg–Li–Al–Ce.

The electrochemical impedance spectra of Mg, Mg–Li–Al–Ce and Mg–Li–Al–Ce–Y electrodes were measured at the open circuit potential after the electrodes were soaked in 0.7 mol L^{-1} NaCl solution for different times. The results are shown in Figs. 4–6, respectively. The capacitive semicircles were observed for all samples. It was found that the diameter of the semicircle, representing the polarization resistance R_p, increases with the soaking time for Mg electrode and decreases with the soaking time for Mg–Li–Al–Ce electrode. However, R_p for Mg–Li–Al–Ce–Y electrode increases firstly and then decreases with the soaking time. The R_p for Mg (ca. 1650 Ω cm^{-2}) is much larger than that for Mg–Li–Al–Ce (ca. 97 Ω cm^{-2}) and Mg–Li–Al–Ce–Y (ca. 150 Ω cm^{-2}) after soaking for

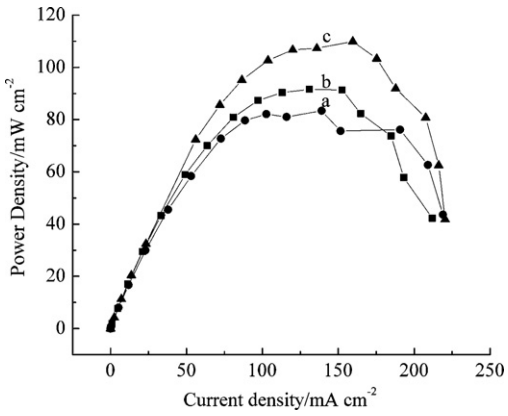

Fig. 9. The plots of the current density vs. power density of metal-H_2O_2 semi fuel cell with (a) Mg, (b) Mg–Li–Al–Ce and (c) Mg–Li–Al–Ce–Y anodes at room temperature. The cathode is nickel foam supported with Pd–Ir catalyst. Anolyte: 0.7 mol L^{-1} NaCl, flow rate: 100 mL min^{-1}. Catholyte: 0.7 mol L^{-1} NaCl + 0.5 mol L^{-1} H_2O_2 + 0.1 mol L^{-1} H_2SO_4, flow rate: 100 mL min^{-1}.

24 h. This result indicates that the Mg electrode is less corrosive than the Mg–Li–Al–Ce and Mg–Li–Al–Ce–Y electrodes. This is in good agreement with the results obtained from Tafel plots (Fig. 1). According to literature [18], the capacitive behavior (i.e. the insulating behavior) may indicate that the Mg surface exhibits better insulating behavior and corrosion resistance than that of Mg–Li–Al–Ce and Mg–Li–Al–Ce–Y surface, that is, the Mg electrode is more passive than the other two electrodes. This might be due to the thick passivation layer on the Mg surfaces produced during the soaking and the passivation may become thick with increase in the soaking time. Thus, the thick passivation layer could prevent the liquid electrolyte from contact with the electrode, leading to the small corrosion current and the good corrosion resistivity. Mg–Li–Al–Ce–Y alloy is more corrosion resistive than Mg–Li–Al–Ce, which can be attributed to the presence of Y. Y may change the alloy structure or assist the formation of an easy-peel-off layer on the alloys surface.

In order to test the electrochemical stability and the activity of the electrodes, the potentiostatic current–time curves at −1.0 V were measured and shown in Fig. 7. The current–time profiles are similar for all the electrodes. The anodic current increases rapidly in the initial stage due to the double layer charging and then reached an approximate constant value. The roughen nature of the curves is due to the repetitive formation and peeling off of the oxidation products [18,24]. The Mg–Li–Al–Ce–Y electrode possesses the highest current density (about 43 mA cm^{-2}) within the measuring period among the three electrodes. The activity increases in the following order: Mg < Mg–Li–Al–Ce < Mg–Li–Al–Ce–Y. All the three electrodes show no sign of decrease in the current within 300 s discharging time. Mg–Li–Al–Ce–Y also exhibits a shortest transition time for the current reaching the stable value among the three electrodes. It can be concluded from the potentiostatic current–time curves that the quinary alloy of Mg–Li–Al–Ce–Y is more active than the quaternary Mg–Li–Al–Ce and Mg. The incorporation of Y element into the quarternary Mg–Li–Al–Ce alloy can activate the alloy and improve its discharging current.

Fig. 8 shows the SEM images of the Mg, Mg–Li–Al–Ce and Mg–Li–Al–Ce–Y before and after immersed in the 0.7 mol L^{-1} NaCl solution for 8 h. It can be observed that after soaking, surfaces of Mg and Mg–Li–Al–Ce–Y show the fine and even crackles, but, the Mg–Li–Al–Ce alloy surface displays much deeper and larger channels. This observation indicated that the Mg and Mg–Li–Al–Ce–Y alloys are more resistive than the Mg–Li–Al–Ce alloy, which is consistent with the results of Tafel plots and the electrochemical impedance spectra.

The Mg–H_2O_2 semi-fuel cell with the Mg, Mg–Li–Al–Ce, and Mg–Li–Al–Ce–Y anodes were assembled and their performances are shown in Fig. 9. The peak power densities for the semi-fuel cells with Mg, Mg–Li–Al–Ce, and Mg–Li–Al–Ce–Y anodes are 83.36, 91.34 and 109.95 mW cm^{-2}, respectively. So, the Mg–H_2O_2 semi-fuel cell with Mg–Li–Al–Ce–Y anode shows the best performance. Its performance is also better than Mg–Li–Al–Ce–Zn (81 mW cm^{-2}) and Mg–Li–Al–Ce–Zn–Mn (91 mW cm^{-2}) anodes reported in the literature [24]. According to the above data, the power densities of the alloys are not much larger compared to pure Mg. However, the relatively few slip systems of hcp Mg alloy at room temperature give it poor workability, and so obtaining a thin anode foil of pure magnesium is difficult. The addition of Li increases the ductility of Mg alloy at room temperature by changing the crystalline structure from hcp Mg to bcc Mg. Therefore the fabrication of alloy anode with different shapes is easier than that of pure Mg anode [21].

4. Conclusions

The electrochemical performances of the Mg–H_2O_2 semi-fuel cells with Mg, Mg–Li–Al–Ce or Mg–Li–Al–Ce–Y anode were investigated. The following conclusions can be obtained from this study:

(1) The Mg and Mg–Li–Al–Ce–Y alloys were more corrosion resistant than Mg–Li–Al–Ce alloy. The corrosion current density of Mg, Mg–Li–Al–Ce and Mg–Li–Al–Ce–Y is 1.3 mA cm^{-2}, 16.8 mA cm^{-2} and 3.5 mA cm^{-2}, respectively. The R_p for Mg, Mg–Li–Al–Ce–Y and Mg–Li–Al–Ce is about 1650, 150 and 97 Ω cm^{-2}, respectively, when the electrodes were soaked in 0.7 mol L^{-1} NaCl solution for 24 h.
(2) Mg–Li–Al–Ce–Y anode is more active than Mg and Mg–Li–Al–Ce anode. Its discharge current density at −1.0 V in 0.7 mol L^{-1} NaCl solution can reach about 43 mA cm^{-2}.
(3) The maximum peak power density of Mg–H_2O_2 semi-fuel cells using Mg, Mg–Li–Al–Ce and Mg–Li–Al–Ce–Y as anodes reached 83.4, 91.3 and 110.0 mW cm^{-2}, respectively.

Acknowledgements

We show gratefully acknowledgment to Dr. Milin Zhang and Zhongyi Niu for the assistance in alloys preparation. This work was financially supported by Natural Science Foundation of Heilongjiang Province of China (B200809), Fundamental Research funds for the Central Universities (HEUCF101023), Key Laboratory of Superlight Material and Surface Technology of Ministry of Education, and Ph.D. Programs Foundation of Ministry of Education of China (20102304110001).

References

[1] D.J. Brodrecht, J.J. Rusek, Appl. Energy 74 (2003) 113–124.
[2] R.R. Bessette, M.G. Medeiros, C.J. Patrissi, C.M. Deschenes, C.N. LaFratta, J. Power Sources 96 (2001) 240–244.
[3] M.G. Medeiros, E.G. Dow, J. Power Sources 80 (1999) 78–82.
[4] S. Ono, K. Asami, T. Osaka, N. Masuko, J. Electrochem. Soc. 143 (1996) 106–109.
[5] W.Q. Yang, S.H. Yang, G.Q. Sun, Q. Xin, Chin. J. Power Sources 29 (2005) 182–186.
[6] W.Q. Yang, S.H. Yang, W. Sun, G.Q. Sun, Q. Xin, Electrochim. Acta 52 (2006) 9–14.
[7] W.Q. Yang, S.H. Yang, W. Sun, G.Q. Sun, Q. Xin, J. Power Sources 160 (2006) 1420–1424.
[8] R.R. Bessette, J.M. Cichon, D.W. Dischert, E.G. Dow, J. Power Sources 80 (1999) 248–253.
[9] M.G. Medeiros, C.G. Zoski, J. Phys. Chem. B 102 (1998) 9908–9914.
[10] Ø. Hasvold, N.J. Størkersen, S. Forseth, T. Lian, J. Power Sources 162 (2006) 935–942.
[11] R.P. Hamlen, D.W. Atwater, in: D. Linden, T.B. Reddy (Eds.), Handbook of Batteries, 3rd ed., McGraw-Hill, 2002, pp. 381–384.
[12] E.G. Dow, R.R. Bessette, M.G. Medeiros, H. Meunier, G.L. Seebach, J. Van Zee, C. Marsh-Orndorff, J. Power Sources 65 (1997) 207–212.

[13] C. Marsh, H. Munier, R. Bessette, M.G. Medeiros, J. Van Zee, G. Seebach, An effective method for the reduction of H_2O_2, US Patent #5,296,429.
[14] A.J. Bard, R. Parsons, J. Jordan, Standard Potentials in Aqueous Solution, IUPAC, Marcel Dekker Inc., 1985.
[15] W. Latimer, Oxidation Potentials, second ed., Prentice Hall, New York, 1953.
[16] M.G. Medeiros, R.R. Bessette, C.M. Deschenes, C.J. Patrissi, L.G. Carreiro, S.P. Tucker, D.W. Atwater, J. Power Sources 136 (2004) 226–231.
[17] M.G. Medeiros, R.R. Bessette, C.M. Deschenes, D.W. Atwater, J. Power Sources 96 (2001) 236–239.
[18] S. Zein, E.L. Abedin, F. Endres, J. Appl. Electrochem. 34 (2004) 1071–1080.
[19] N.A. Popovich, R. Govind, J. Power Sources 112 (2002) 36–40.
[20] A. Sivashanmugam, T.P. Kumar, N.G. Renganathan, S. Gopukumarl, J. Appl. Electrochem. 34 (2004) 1135–1139.
[21] M.C. Lin, C.Y. Tsai, J.Y. Uan, Corros. Sci. 51 (2009) 2463–2472.
[22] D.X. Cao, X. Cao, G.L. Wang, L. Wu, Z.S. Li, J. Solid State Electrochem. 14 (2010) 851–855.
[23] D.X. Cao, L. Wu, Y. Sun, G.L. Wang, Y.Z. Lv, J. Power Sources 177 (2008) 624–630.
[24] D.X. Cao, L. Wu, G.L. Wang, Y.Z. Lv, J. Power Sources 183 (2008) 799–804.